ACS APPLIED MATERIALS & INTERFACES

www.acsami.org

Research Article

Understanding the Role of Oxidative Debris on the Structure of Graphene Oxide Films at the Air−Water Interface: A Neutron Reflectivity Study

David López-Díaz, M. Dolores Merchán, M. Mercedes Velázquez,* and Armando Maestro*

Cite This: *ACS Appl. Mater. Interfaces* 2020, 12, 25453−25463

Read Online

ACCESS | Metrics & More | Article Recommendations

ABSTRACT: We address here the role of oxidation impurities on the structure of graphene oxide films at the air−water interface by specular neutron reflectivity (SNR). We study films of purified graphene oxide (PGO) and nonpurified graphene oxide in the close-packed state. Nonpurified graphene oxide is constituted by graphene oxide (GO) layers with oxidation impurities adsorbed on the basal plane, while in PGO sheets, impurities are eliminated. SNR measurements show that GO films are formed by well-defined bilayers constituted by 2−3 layers of GO stacked in contact with air and a second layer of impurities submerged in the aqueous subphase. In contrast, PGO films are formed by a single layer in contact with air. We show for the first time that impurities constitute a layer submerged in the aqueous subphase, decrease the elasticity, and favor the collapse of graphene oxide films. Our results allow designing the surface properties of GO trapped at fluid interfaces.

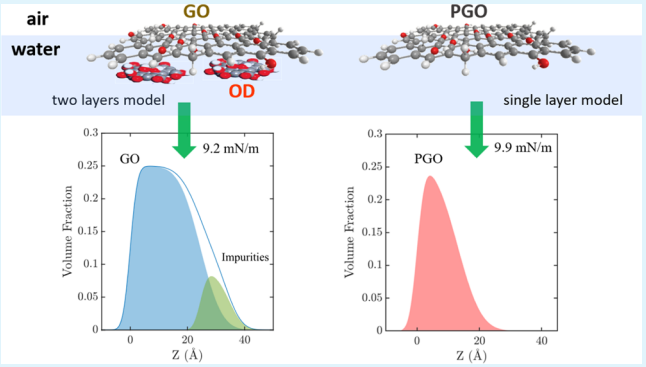

KEYWORDS: *graphene oxide, purified graphene oxide, oxidative debris, Langmuir films, neutron reflectivity*

INTRODUCTION

Graphene is a 2D layer of sp^2-hybridized carbon atoms, arranged in a hexagonal lattice. Because of its extraordinary properties, it has been suggested as a promising component for transparent conducting electrodes,[1] transistors,[2] hydrogen storage,[3] CO_2 capture,[4] and gas sensors.[5] However, each application requires a different set of properties. Thus, for electronic applications, graphene obtained by mechanical exfoliation of graphite or by chemical vapor deposition (CVD) render good quality sheets; however, because of the absence of functional groups, these materials cannot be used in applications such as sensors, inks, or in biomedical applications such as bioimaging or in drug delivery vectors. In these applications, graphene oxide presents several advantages against graphene because it contains oxygen functional groups which can bind polymers or nanoparticles to modulate the properties of new hybrids according to the needs of each application.[4,6] Besides, the O-groups render aqueous dispersibility to graphene oxide, this being an important property in several applications.[7−10]

Graphene oxide (GO) is synthesized by oxidation[11] of graphite or carbon nanofibers through different synthetic routes, including two of the most widely used, the Staudenmaier[12] and Hummers[13] methods. The chemical structure of graphene oxides thus obtained is still subject to debate due to its strong dependence on the synthesis route and the precursors used for oxidation.[14] However, although the oxidation degree and the nature of O-groups differ depending on the oxidation protocols and the starting materials, there is an agreement on the localization of O-groups. Over the last decades, the most commonly assumed model[15,16] considers that the carboxylic and ketone groups are mainly situated at the edges of sheets, whereas basal planes are functionalized by 1,2 epoxy and hydroxyl groups. An important issue for several applications is to achieve the most suitable oxidation degree for each application that is usually achieved by total or partial reduction of graphene oxide. Reduction by chemical agents or thermal annealing decreases the oxidation degree of graphene oxide, although the graphene structure is not completely restored. In the chemical reduction, the oxidized groups of reducing agents often remain attached to the basal plane,[17] modifying the properties of graphene oxide. High-temperature

Received: March 26, 2020
Accepted: May 12, 2020
Published: May 12, 2020

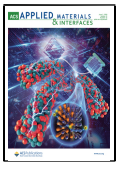

https://dx.doi.org/10.1021/acsami.0c05649
ACS Appl. Mater. Interfaces 2020, 12, 25453−25463

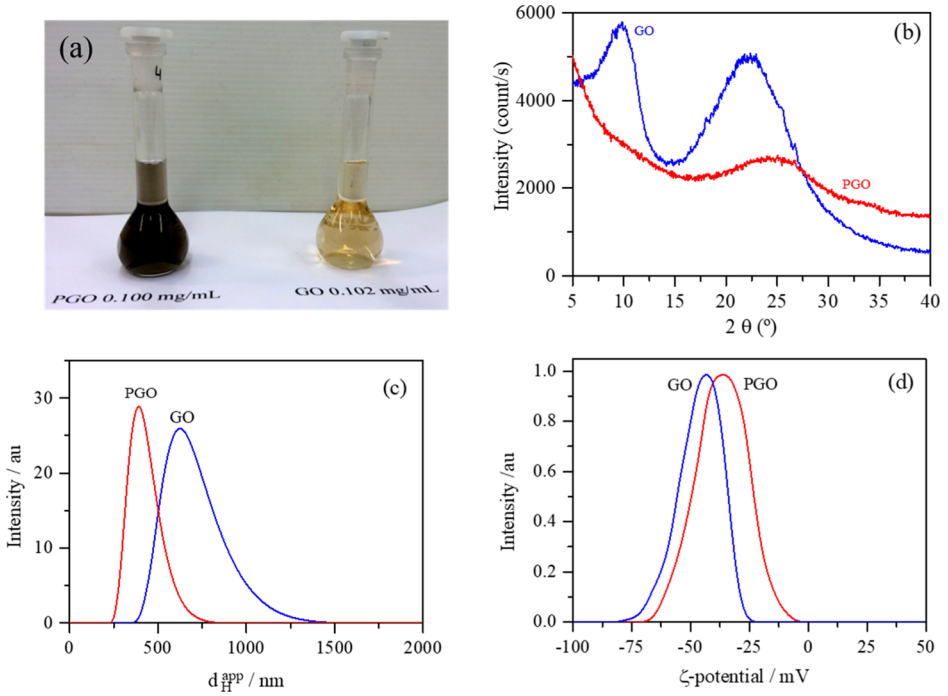

Figure 1. (a) Water dispersions of GO and PGO. (b) XRD diffractograms of GO and PGO. (c) Size distribution peaks. (d) ζ-Potential measurements of aqueous solutions of GO and PGO.

annealing (>750 °C) is the method that can remove almost all O-groups;[18] however, if the temperature is quickly increased, some defects or vacancies are created and the graphene oxide network gets damaged.[19,20] In the last years, an alternative method has been reported. The method consists of GO purification by alkaline washing.[21] Oxidation by concentrated acids was showed to produce highly oxidized low molecular weight fragments referred as oxidative debris (OD). They consist of mixtures of oxidized polyaromatic fragments adsorbed on GO nanoplatelets and can be removed by base washing.[20,21] After washing, the purified graphene oxide (PGO) presents oxidation degree values as obtained by chemical reduction.[21]

The existence of OD has important effects on GO properties. Thus, the elimination of OD increases the conductivity of GO by 5 orders of magnitude[21] and also modifies its catalytic activity.[22] Besides, impurities increase the water dispersibility of GO and modify the spectroscopic properties of GO dispersions.[23] In this sense, the luminescence of GO was attributed to OD molecules because PGO is not a fluorescent material.[24] The origin of OD was questioned in a recent work.[25] The authors contested the two-component model of GO, sheets of GO and OD attached at the GO sheets, and postulated that the purified GO is mainly made up of small graphene oxide platelets obtained by cutting C−C bonds during alkaline treatment.[25] The origin and location of OD are still debated, probably because of the difficulty of detecting OD by microscopy or spectroscopic techniques. However, the location of OD on GO sheets was recently analyzed by the adsorption isotherms of phenanthrene and dinitro benzene and the results seem to confirm the two-component model. Results also point to π stacking as the origin of OD/GO interactions.[26]

One aspect poorly studied so far is the effect of impurities on GO films at the air−water or air−solid interfaces. Because of their hydrophobic and hydrophilic domains, GO sheets have been considered as surfactant material and form stable Langmuir monolayers at the air−water interface[27,28] when GO sheets dissolved in water/methanol mixtures are spread on the acidic aqueous interface.[17,29−31] The possibility of preparing stable Langmuir monolayers of GO is very interesting to build GO films on solid wafers through the Langmuir−Blodgett (LB) or Langmuir−Schaeffer (LS) methodologies. These methodologies consist of the process of transferring Langmuir monolayers from the air−water interface to a solid wafer by vertical (LB) or horizontal (LS) dipping of the solid in the Langmuir monolayer.[32] They were designed to avoid undesirable aggregation of sheets or the formation of heterogeneous domains usually produced by other deposition methodologies, such as drop-casting[33] and spin-coating.[34]

In the last years, by the Langmuir−Blodgett[17,27,28,30,35] or Langmuir−Schaefer[31] methodologies, films of GO have been constructed; however, little attention has been paid to the role of OD in the structure of these films. In a recent work, we have studied this effect showing that the solid coverage of unpurified films was always higher than that of purified films.[30,31] We believe that this behavior could be due to the different orientation and organization of purified and non-purified graphene oxides in the Langmuir monolayer precursor of the LB and LS films. Therefore, to interpret this fact, the deep knowledge of the orientation and the organization of graphene oxide sheets at the air−water interface is necessary. To this end, we consider that specular neutron reflectivity (SNR) is the most suitable technique to study the composition and structure of complex systems adsorbed on a fluid interface in the direction perpendicular to its plane.[36−38] Neutron diffraction and inelastic neutron scattering measurements have been performed to study the structure of GO and reduced graphene oxide (rGO).[39,40] Results showed stacking structures of different lateral dimensions and interlayer distances for GO and rGO. On the other hand, neutron

https://dx.doi.org/10.1021/acsami.0c05649
ACS Appl. Mater. Interfaces 2020, 12, 25453−25463

reflectivity measurements of GO thin films deposited on Si wafers were used to evaluate the amount of solvents sandwiched in GO films and to study the selectivity in sorption of solvents from binary mixtures.[41] In a recent work,[42] Bonatout et al. studied the structure of graphene oxide films at the air−water interface using X-ray reflectivity (XRR) and grazing incidence X-ray diffraction[42] (GIXD). They showed that GO films at the water interface are constituted by a bilayer of GO sheets that have different roughness, density, and thickness; the bilayer exists at low and high surface densities.[42] However, to the best of our knowledge, there is no single study so far, comparing the structure of graphene oxide and PGO at the air−water interface. Therefore, the effect of oxidation impurities (OD) on the structure of GO films at the air−water interface is not sufficiently understood.

Based on this framework, the main objective of the current work is to study the effect of oxidation impurities on the orientation and specific organization of GO sheets in films at the air−water interface by combining SNR and surface tensiometry experiments. The selected materials were graphene oxide synthesized by oxidation of graphite flakes and PGO, obtained by alkaline washing of the graphene oxide. Our results show significant differences between the film structures of these materials. According to our experiments, GO films consist of a bilayer of graphene oxide in contact with air and a second layer of oxidation impurities submerged in the aqueous subphase. When impurities were removed by base washing, the PGO films were elucidated using a single layer pinned at the water interface.

EXPERIMENTAL SECTION

Sample Preparation. GO was obtained by oxidation of natural graphite flakes (Qingdao Super Graphite Co., Ltd.; 99.02 fixed C) using a modified Hummers' method developed by our group[14,17,31] to obtain highly oxidized GO sheets of a few layers. Besides, in the current work, we have modified the procedure to obtain high-quality GO sheets using successive filtrations of the GO dispersions through sieves of a mesh size of 0.425, 0.090, and 0.020 mm. The size and superficial electric charge of sheets were determined by light scattering and ζ-potential measurements, respectively.

The purification process was reported by Rourke[21] and was previously used by our group to purify different kinds of graphene oxide.[14,30,31] In brief, graphene oxide was dispersed in water (0.1 mg·mL^{-1}) by sonication during 10 min in an ultrasound bath. Then, 1 mL of 1 M NaOH solution was added dropwise to 50 mL of graphene oxide dispersion until the solution changed the color from brown to black. The solution is heated under reflux for 1 h and then the purified graphene oxide solution is neutralized under reflux with HCl (1 M) for at least 1 h. The solution thus obtained was centrifuged at 1900g for 5 min, and the supernatant solution of oxidation impurities was discarded. The solid material was washed with water until the salts produced during neutralization were removed. Black aggregates of PGO were dispersed in water by sonication. PGO dispersions present black color due to the low oxidation degree, whereas GO dispersions are brown due to their higher oxidation degree, see Figure 1a.

The reagents used for GO synthesis and purification were: $NaNO_3$ (99%), H_2SO_4 (98% w), $KMnO_4$ (>99%), H_2O_2 (30% w), NaOH, and HCl (35%). They were provided by Sigma-Aldrich (St. Louis, MO, USA) and used without further purification. Methanol (HPLC >99.9%) used for spreading solution was also provided by Sigma-Aldrich (St. Louis, MO, USA). For SNR experiments, deuterated water (isotopic purity > 99.9 wt %) was provided by Sigma-Aldrich (St. Louis, MO, USA). Millipore Ultrapure water prepared using a combination of RiOs and Milli-Q systems from Millipore was used to prepare GO solutions, reactions, and the subphase in the Langmuir trough. The conductivity of the water was lower than 0.2 μS/cm, and its surface tension value was 72.5 mN m^{-1}.

Experimental Methods. The pressure-area isotherms of GO and PGO were recorded on a Langmuir Minitrough (KSV, Finland) placed on an antivibration table. The spreading solutions, 0.65 mg mL^{-1} for GO and 0.17 mg mL^{-1} for PGO, were dissolved in water/methanol mixtures (1:5 v/v), as it was proved to be a good spreading solvent for graphene oxide.[27] They were deposited on the subphase of slightly acidic water with a Hamilton micrometer syringe with an accuracy of 1 μL. The volume of solution spread at the air−water interface was 2.5 mL for the GO solution (0.65 mg mL^{-1}) and 5.0 mL for PGO (0.17 mg mL^{-1}). The pH of the aqueous subphase was adjusted to 1.5−2 using a 1 M HCl solution. We selected this pH because we previously demonstrated that at this pH, these materials containing acid groups are in their nonionic form and, as a consequence, are irreversibly pinned at the interface.[31]

The surface pressure was measured with a paper plate (Whatman CHR1 chromatography paper) connected to an electrobalance. The subphase temperature was maintained at 20.0 ± 0.1 °C by making thermostated water flow through jackets at the bottom of the trough. The temperature at the surface was measured with a calibrated KSV sensor, while the water temperature was controlled by the Lauda Ecocline RE-106 thermostat/cryostat.

X-ray photoelectron spectra of powder samples were measured in a VG Escalab 200R spectrometer (Fisons Instruments, Parkton, MD, USA). The equipment uses an excitation source of Mg Kα ($h\nu$ = 1253.6 eV) radiation and a hemispherical electron analyzer. High-resolution spectra were recorded at 20 eV analyzer pass energy. The residual pressure in the analysis chamber was kept under 4×10^{-7} Pa during data acquisition.

Powder XRD patterns were recorded in a Bruker D8 Advance powder diffractometer (Bruker Corp., Billerica, MA, USA) using Cu Kα1,2 radiation (λ = 1.54050 Å) between 5 and 40° (2θ) with a step size of 0.05° and a step time of 2.6 s. The tube was operated at 40 kV and 30 mA.

Dynamic light scattering (DLS) and ζ potential measurements were carried out on a Zetasizer Nano ZS device (Malvern Instruments, Malvern, UK). We use graphene oxide solutions of two different concentrations: 0.10 and 0.05 mg·mL^{-1} for GO and PGO, respectively. For ζ-potential experiments, the electrophoretic mobility was measured at 20.0 °C using a DTS 1060C disposable cell. The electrophoretic mobility, μ_e, was converted in ζ-potential using the Smoluchowski relationship,[43] $\zeta = \eta\mu_e/\varepsilon$, where η and ε represent the absolute viscosity and permittivity of water at 20 °C, respectively.

DLS experiments were also performed at 20.0 °C. The intensity autocorrelation functions were obtained at 13° and transformed into electric field autocorrelation functions according to the Siegert relationship. We have used DLS measurements to estimate the size of nanoplatelets because we have previously reported that the estimated values using this methodology acceptably agree with the size values obtained from scanning electron microscopy (SEM) images.[31]

SNR Experiments. Reflectivity (R) is defined as the ratio of neutrons scattered from the interface over the incident intensity of the neutron beam. Specular reflection means that the incident angle of the neutron beam is equal to the reflected angle (θ). Routinely, a reflectivity profile in specular conditions is obtained by measuring R as a function of the momentum transfer vector $Q = \frac{4\pi}{\lambda}(\sin\Theta)$, normal to the interface, where λ is the wavelength of the neutron beam. The measured $R = R(Q)$ profile of a structured interface is usually linked to a plane-averaged scattering length density (SLD) profile perpendicular to the interface.[44] SLD measures the coherent scattering cross-section of the molecular species that constitutes each interfacial layer and is linked to their chemical composition and molecular volume, V, by

$$\mathrm{SLD} = \frac{1}{V}\sum_i b_i n_i \quad (1)$$

where n_i is a number density and b_i is the SLD of each molecular species.

https://dx.doi.org/10.1021/acsami.0c05649
ACS Appl. Mater. Interfaces 2020, 12, 25453−25463

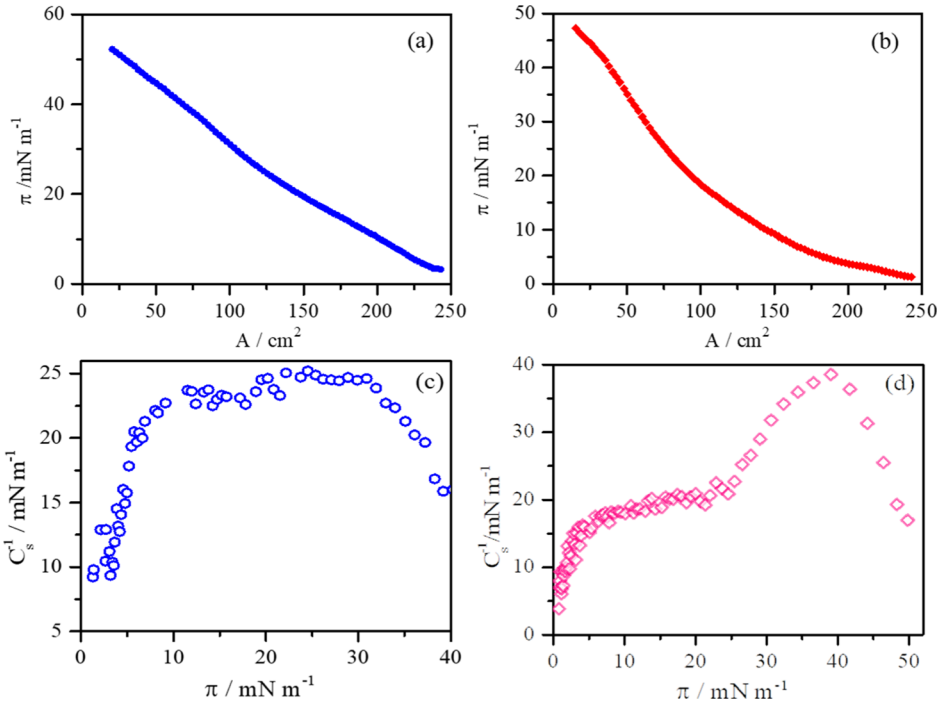

Figure 2. Surface pressure-area isotherms recorded at 20 °C for (a) GO and (b) PGO. Variation of the surface compressional elastic modulus with the surface pressure for GO (c) and PGO (d) films.

SNR measurements were performed on FIGARO, a time-of-flight reflectometer, at the Institut Laue-Langevin (Grenoble, France). Two angles of incidence, θ = 0.62 and 3.8° and a wavelength resolution of 7% dλ/λ were used, yielding a momentum transfer range of 0.005 < Q < 0.3 Å^{-1} and a residual background reflectivity of $R \approx 10^{-7}$. Measurements were performed in two isotopic contrasts: pure D_2O and a mixture of 8.1% v/v D_2O/H_2O called air-contrast matched water (ACMW) that has a SLD of zero. The raw time-of-flight experimental data at these two angles of incidence are routinely calibrated with respect to the incident wavelength distribution and the efficiency of the detector, yielding the resulting $R(Q)$ profile using COSMOS.[45] SNR data modeling was performed by minimizing the difference between the experimental and the calculated reflectivity profile. The latter was obtained by a model consisting of one or two layers of constant SLD using the Parratt's recursive formalism,[46] with an error function connecting adjacent layers, to describe the interfacial constraints between layer parameters (thickness, roughness, SLD, and volume fraction). Data analysis was performed using Aurore software.[47] We exploit the SLD contrast variation method to reduce the ambiguity of data modeling for determining the thickness, roughness, and the degree of hydration of the interfacial layers between the air and the bulk. Therefore, we fitted simultaneously reflectivity data sets measured in two isotopically different bulk solvent phases (contrasts), such as D_2O and ACMW, with a global minimization of a least-squares function, χ^2 to obtain the best set of global parameters for each layer.

RESULTS AND DISCUSSION

Prior to the preparation of Langmuir monolayers, we characterize the materials by X-ray photoelectron spectroscopy (XPS), X-ray diffraction (XRD), DLS, and ζ-potential measurements.

To quantify the percentage of O groups attached at the graphene oxide sheets, we have recorded the X-ray photoelectron spectra of GO and PGO. Results showed that the C/O ratio increases from 1.46 to 4.9 after GO purification by alkaline washing. These values are in good agreement with those previously reported for these materials.[14,21,31]

XRD measurements were made to analyze the crystallinity of materials. Results are plotted in Figure 1b. The diffractogram of GO presents two main features at 2θ values of 10° (peak I) and 22° attributed to (002) reflection. These peaks were observed in the XRD spectrum of graphene oxide synthesized from graphite[48] and could be due to oxidative impurities or other kinds of defects.[20,30] In the diffractogram of PGO, the peak I disappears, whereas the main peak is centered at 25°. The disappearance of the peak at 10° was observed for graphene oxides annealed at temperatures above 200 °C and is signature of the decrease in the degree of oxidation.[20] Besides, the (002) peak is shifted from 22 to 25° after GO purification. From 2θ position using the Bragg's law, the interlayer distance, d_{002}, can be calculated. The d_{002} values change from 0.4 to 0.347 nm when GO was purified. The interlayer distance value for PGO (0.347 nm) is close to the value corresponding to pristine graphene (0.34 nm).[49] Our results show that d_{002} decreases after GO purification by alkaline washing. This behavior was previously observed for graphene oxides synthesized by oxidation of carbon nanofibers[30] and is due to the removal of small fragments of highly oxidized materials, that is OD.

Finally, we also obtain the nanoplatelet size and the surface electric charge using DLS and the ζ-potential measurements, respectively. Results are plotted respectively in Figure 1c,d.

As can be seen in Figure 1c, the size distribution functions are monomodal for the two materials and the apparent hydrodynamic diameter values obtained for GO and PGO sheets were 615 ± 8 and 376 ± 5 nm, respectively. This means that the purification procedure generates smaller sheets. This behavior was previously reported and was attributed to breaking of the sheets by sonication used to disperse the purified material[50] or to the elimination of impurities adsorbed onto the basal plane.[31] On the other hand, the ζ-potential

https://dx.doi.org/10.1021/acsami.0c05649
ACS Appl. Mater. Interfaces 2020, 12, 25453−25463

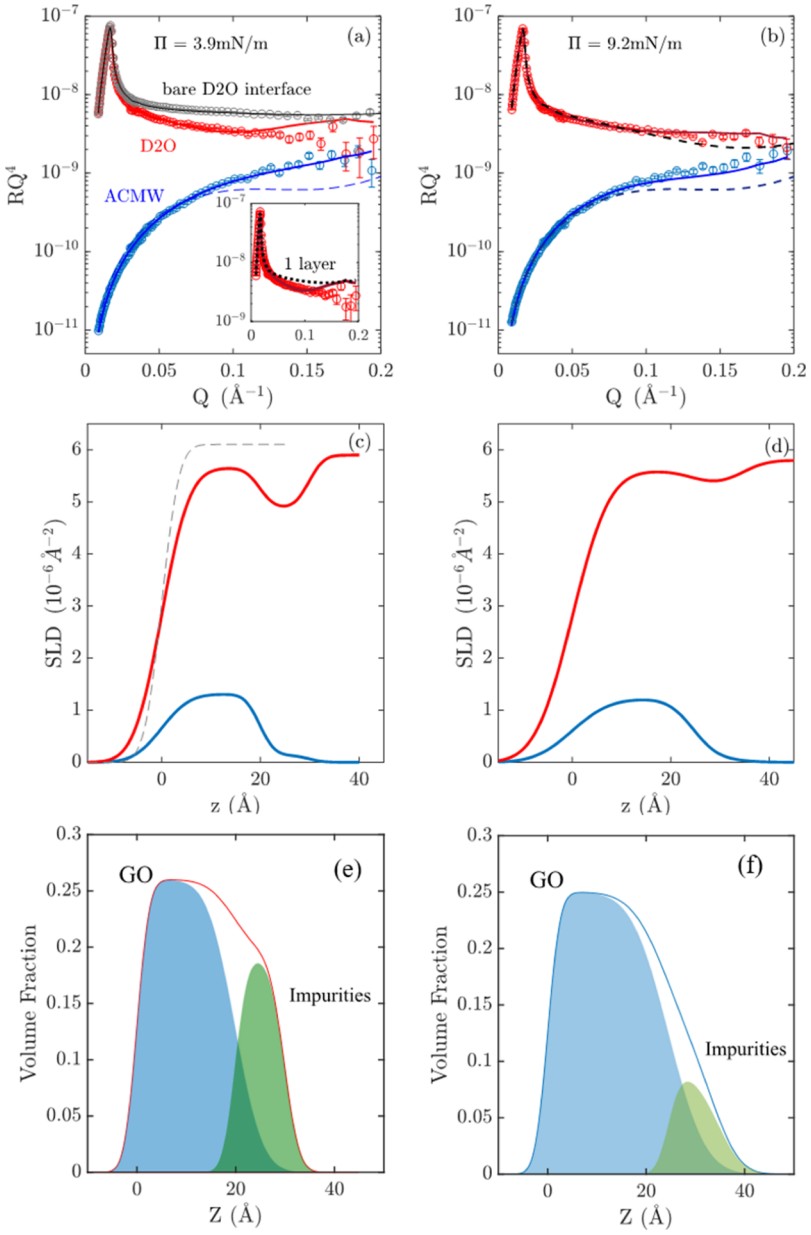

Figure 3. Experimental (symbols) and simulated (lines) reflectivity profiles of GO films at the surface pressure values of 3.9 mM/m (a) and 9.2 mN/m (b). The reflectivity profile corresponding to a bare air/D_2O interface and the fitting were included in (a). Dotted lines in (a,b) are simulated curves calculated according to a single-layer model and solid lines in (a,b) are simulated curves calculated according to a 2-layer model and the parameter listed in Table 1. The inset in (a) is a magnification of the reflectivity profile and simulated curves for the reflectivity profile of GO in pure D_2O contrast. Scattering length profiles corresponding to fits are plotted in (c,d). SLD profile corresponding to bare D_2O interface is also plotted in (c) as dotted line. Symbols and lines in red correspond to measurements in pure D_2O contrast and blue symbols and lines to ACMW contrast. Variation of the total volume fraction and the two corresponding layers (GO and impurities) with the distance to the air−water interface z of GO films at the surface pressure values of 3.9 mM/m (e) and 9.2 mN/m (f).

values of GO and PGO aqueous solutions show monomodal functions centered at −43 and −36 mV, respectively.

We compare these results with those reported for GO and PGO. Concerning the diameter of the sheets, the values determined in the current work are smaller than those previously reported,[14,31] 825 nm (GO) and 712 nm (PGO). On the other hand, the ζ-potential value obtained for PGO is in excellent agreement with the previously measured value for this material (−34 mV).[31] In contrast, the ζ-potential obtained in the previous work for GO is a bimodal function with two maxima at −42 and −65 mV;[31] therefore, the ζ-potential value found in the current work for GO agrees very well with the one previously reported for the population with low surface charge. To interpret the differences observed between the dimensions of GO and PGO previously reported and those obtained in the current work, it is necessary to consider that the procedures employed to separate the sheets of high quality from the solutions of GO were different. Thus, we used centrifugation in our previous work,[30,31] whereas in the current work, we have made three successive filtrations with sieves of different mesh sizes. In view of all results, it is possible to conclude that filtration renders smaller sheets than centrifugation. Concerning the surface electric charge, in the case of GO, the filtration procedure renders sheets with a monomodal distribution.

https://dx.doi.org/10.1021/acsami.0c05649
ACS Appl. Mater. Interfaces 2020, 12, 25453−25463

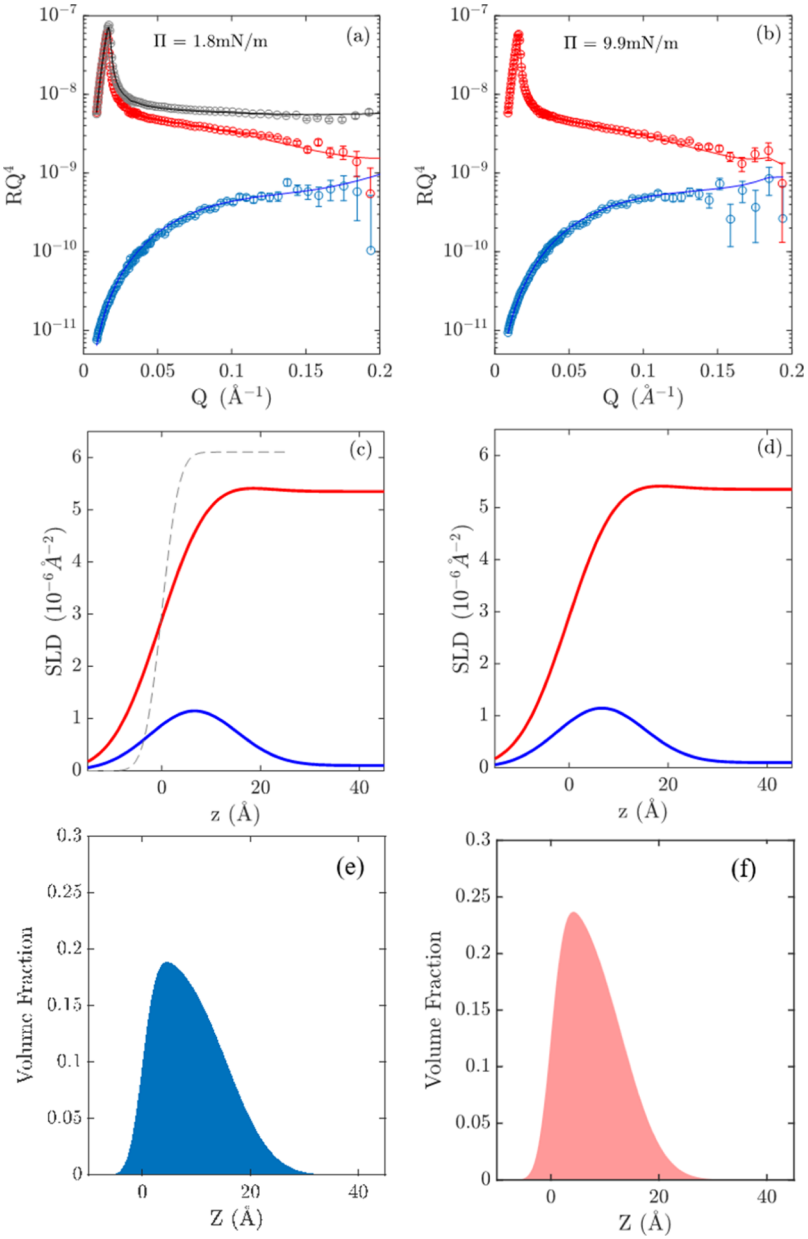

Figure 4. Experimental (symbols) and simulated (lines) reflectivity profiles of PGO films at the surface pressure values of 1.8 mM/m (a) and 9.9 mN/m (b). The reflectivity profile corresponding to a bare air/D_2O interface, including the fitting (line) were plotted in (a). Simulated curves are obtained according to a single layer model and the parameters listed in Table 2. Scattering length profiles corresponding to fits are shown in (c,d). Symbols and lines in red correspond to measurements in pure D_2O contrast and blue symbols and lines to ACMW contrast. Variation of volume fraction with the distance to the air−water interface for PGO films at the surface pressure of 1.8 (e) and 9.9 mN/m (f), respectively.

Finally, the electric charge of purified graphene oxide is lower than that of the unpurified material. This fact has been previously reported[30,31] and is consistent with the removal of highly oxidized fragments functionalized with carboxyl groups during the purification procedure.[50]

Graphene Oxide Langmuir Films. We have recorded the surface pressure-area isotherms of GO and PGO in Figure 2a,b, respectively. Figure 2c,d displays the surface compressional elastic modulus, C_s^{-1}, calculated from the surface pressure isotherms and the following equation

$$C_s^{-1} = -A\left(\frac{\delta\pi}{\delta A}\right)_{p,T} \quad (2)$$

where π and A represent the surface pressure and area, respectively.

The surface pressure and the compressional elastic modulus isotherms are quite similar to those previously reported for GO and PGO;[27,31] therefore, we interpret them in a similar way. Accordingly, the monolayers at the surface pressure and compressional modulus close to zero are assigned to isolated GO sheets.[27,29−31] As the surface pressure increases, the sheets approach each other, increasing the surface pressure and the compressional elastic modulus into a close-packed region. AFM and SEM images taken in this region show that the gaps between GO sheets are small.[27] Beyond the close-packed region, when the film is further compressed, SEM images revealed that the GO sheets fold at the touching points.[27] As

https://dx.doi.org/10.1021/acsami.0c05649
ACS Appl. Mater. Interfaces 2020, 12, 25453−25463

was previously reported,[27] at this stage the surface pressure moderately increases. At higher pressures, two different behaviors are observed, for the GO film, the compressional elastic modulus decreases, whereas for the PGO, the compressional elastic modulus increases until it reaches a maximum value. The decrease of the compressional elastic modulus was previously reported and attributed to the collapse.[27] As can be seen in Figure 2c,d, the collapse is observed in both isotherms above a given surface concentration; however, in the PGO isotherm, before the collapse, another region was observed where both the surface pressure and the compressional elastic modulus increase over compression. This region has been reported in some type of graphene oxides,[27] and SEM images showed a nearly complete monolayer of interlocked GO sheets with wrinkles. This layer leads to the monolayer collapse after further compression. We believe that differences between the GO and PGO isotherms could be related to a different organization and orientation of the materials at the air−water interface due to the presence of OD in GO films. Specular neutron reflectivity is a suitable technique to study the structure and composition of thin films in the direction perpendicular to the plane of the interface; therefore, we use this technique to understand the behavior of these materials trapped at the fluid interface.

Neutron Reflectivity Measurements of Graphene Oxide Thin Films. SNR measurements were done to study the film structure of selected monolayers with different surface pressure values in the LE region. We choose films in the close-packed region because at this surface state sheets do not fold or interconnect. To establish an adequate comparison between the behavior of the two materials, we have selected films with the same compressional elastic modulus value. Accordingly, we have selected films at the surface pressure values of 3.9 and 9.2 mN/m for GO and 1.8 and 9.9 mN/m for PGO. At low surface pressure values, the compressional modulus value remains constant at 11 mN/m, whereas at the highest surface pressure values, the compressional modulus value is 21 mN/m. For each monolayer, the reflectivity profiles were recorded throughout the accessible Q-range in two isotopic contrasts: D_2O and ACMW. We also consider that the samples studied here yielded laterally homogeneous interfaces on the length scale of the in-plane neutron coherence length, on the order of several microns. This implies that the measured SNR can be correlated with the averaged SLD depth profile across the interfacial area delimited by this coherence length.

For reference, the measurement of the bare air/D_2O interface is shown in Figures 3a and 4a, including a fit to the data corresponding to a roughness σ_A of 2.8 Å in agreement with the theoretical value expected for thermally excited capillary waves ($\sim\sqrt{k_BT/\gamma_0}$), with γ_0 being the interfacial tension of the bare D_2O interface.[51,52]

The first attempt to fit the reflectivity profile of GO films with a one-layer model of single SLD did not yield a satisfactory correlation with the experimental data as shown in Figure 3a,b. In detail, dotted lines represent the best one-layer model fitting curve with a fixed SLD = 4.96 10^{-6} Å^{-2}, which corresponds to a GO layer. The SLD value was calculated from eq 1, the density value taken of graphene oxide was 1.8 g/cm^3, and the following was the GO composition:[40] C (56.2%), H (0.7%) and O (40.5%) compatible with our XPS results. The best fit of the reflectivity profiles of GO films corresponded to a two-layer model, as shown in Figure 3a,b. This fact agrees very well with results obtained from X-rays surface scattering.[42] In detail, our model is based on a first layer in contact with air and a second one submerged in the aqueous subphase. We consider that the second layer consists of oxidation impurities with an SLD value of 0.68 10^{-6} Å^{-2} calculated from eq 1 and the chemical composition of $C_{19}H_{35}O_6$ and $C_{18}H_{33}O_9$ (1:1) previously reported for oxidation impurities and obtained by high-resolution mass spectrometry.[21] The density used was 1.1 g/cm^3. This value was taken from ref 42 and corresponds to the density of the submerged layer used to interpret X-rays surface scattering data. For the top layer, GO in contact with air, the SLD value used for fitting was SLD_1 = 4.96 10^{-6} Å^{-2}.

The resulting SLD profiles across the interface for GO films at 3.9 and 9.2 mN/m are plotted in Figure 3c,d, respectively. The parameters obtained from the fits are collected in Table 1.

Table 1. Parameters Obtained from the Fits for GO Films[a]

π = 3.9 mN/m		π = 9.2 mN/m	
σ_0/Å	4.4 ± 0.1	σ_0/Å	5.9 ± 0.1
t_1/Å	20.0 ± 0.6	t_1/Å	24.5 ± 0.6
SLD_1/Å^{-2}	4.96 × 10^{-6}	SLD_1/Å^{-2}	4.96 × 10^{-6}
ϕ_{w1}	0.74 ± 0.01	ϕ_{w1}	0.75 ± 0.01
σ_1/Å	2.8 ± 0.5	σ_1/Å	4.0 ± 0.8
t_2/Å	10.0 ± 1.0	t_2/Å	10.0 ± 1.0
SLD_2/Å^{-2}	0.68 × 10^{-6}	SLD_2/Å^{-2}	0.68 × 10^{-6}
ϕ_{w2}	0.81 ± 0.04	ϕ_{w2}	0.91 ± 0.01
σ_2/Å	2.8 ± 0.5	σ_2/Å	4.0 ± 0.8

[a]Errors are reported as absolute values calculated in 1σ interval.

Using these parameters, the variation of the volume fraction, $\Phi(z)$, with the distance to the interface, was calculated using the difference of two error functions as follows

$$\Phi_{GO}(z) = \begin{cases} \frac{1}{2}\phi_{GO,1}\left[\mathrm{erf}\left(\frac{z-\frac{t_1}{2}}{\sqrt{2\sigma_0}}\right) - \mathrm{erf}\left(\frac{z+\frac{t_1}{2}}{\sqrt{2\sigma_1}}\right)\right], & 0 < z < t_1 \\ \frac{1}{2}\phi_{OD,2}\left[\mathrm{erf}\left(\frac{z-\frac{t_2}{2}}{\sqrt{2\sigma_1}}\right) - \mathrm{erf}\left(\frac{z+\frac{t_2}{2}}{\sqrt{2\sigma_2}}\right)\right], & t_1 < z < t_2 \end{cases} \quad (3)$$

where, $\phi_{GO,1} = 1 - \phi_{w1}$ and $\phi_{OD,2} = 1 - \phi_{w2}$ represent the volume fraction of GO and OD in layers 1 and 2, respectively; and ϕ_{wi} represents the resultant fraction of water in each i-layer. The volume fraction values thus calculated are plotted against the distance at the interface in Figure 3e,f.

Parameters in Table 1 show that the properties of the two layers are remarkably different. The top layer consists of GO sheets in contact with air and has a fraction of water in the layer, ϕ_{w1} = 75%. Besides, the thickness of the top layer varies from 20 to 24.5 Å, for films at 3.9 and 9.2 mN/m, respectively. The thickness obtained from the fit for the film at 3.9 mN/m is consistent with thickness of the GO film deposited by LB on Si at the same surface pressure, (20 Å).[17] Based on the reported interlayer distance for GO, 7.93 Å,[41] the layer in contact with

https://dx.doi.org/10.1021/acsami.0c05649
ACS Appl. Mater. Interfaces 2020, 12, 25453−25463

air is constituted by 2−3 GO monolayers. The roughness of the top layer, σ_0, increases from 4.4 to 5.9 Å when the surface pressure increases from 3.9 to 9.2 mN/m. These values agree very well with those previously reported and obtained by X-ray surface scattering for the top layers of GO Langmuir films at the same surface pressure values.[42] Significantly, the observed roughness values for GO layers at both surface pressures far exceed the values originated solely by the presence of capillary waves. For example, at the highest value of interfacial tension, γ, studied here ($\gamma = \gamma_0 - \pi = 63$ mN/m), where γ and π represent the surface tension of water and the surface pressure of the film, the expected capillary roughness, calculated as $\sigma = \sigma_A(\gamma_0/\gamma)^{1/2}$, yields a value of 3.1 Å. Therefore, we consider that the presence of GO layers produces additional apparent roughness due to the molecular protrusions and orientations at the air/water interface that clearly evolve with the reduction in the interfacial area per molecule. With respect to the submerged layer, its thickness, 10 Å, is the same at both pressures and also compared to the value found by Bonatout et al. using X-ray surface scattering for this layer.[42]

The water fraction in the submerged layer increases up to 81−91% compared with the top layer. The increase in the water density on the bottom layer is consistent with the presence of OD molecules more hydrophilic than GO. In addition, the roughness values are also in agreement with the value found for Bonatout.[42] Here, the increase of the roughness of the submerged layer at increasing surface pressure is explained again not only by the presence of capillary waves, but also with a possible change of orientation, or even with the exclusion of some impurity molecular species.

The volume fraction profile for the GO layers in the close-packed state shows two separate distributions (Figure 3e,f). The first corresponds to a distribution of GO sheets in contact with air. This distribution increases when compressing up to 9.2 mN/m as expected for a decrease of the available molecular area. The second distribution corresponds to the oxidation impurities that clearly decreased when reducing the interfacial area. This fact indicates the solubilization of some impurities in the bulk.

In summary, the structural parameters obtained in the current work using SNR agree very well with the results previously obtained by X-ray surface scattering for unpurified graphene oxide films at the air−water interface. It is interesting to note that in our model the structural parameters of the layer submerged in the aqueous subphase have been calculated using the SLD value corresponding to the chemical composition of the oxidation impurities, OD. In addition, if we compare the thickness of OD obtained by fitting the SNR results, 1 nm, with the value recently determined by AFM, 0.5−1.5 nm,[26] the two values are in very good agreement. All these facts are strong arguments that support the nature of the bottom layer on GO films. According to our results, the submerged layer is mainly constituted by small fragments of highly oxidized material produced during the oxidation of graphite. Finally, the SNR results also show that the volume fraction of the OD layer is smaller than the volume fraction of the GO sheets. This is an expected result considering that the mass attributable to OD is around 30% of the total mass of unpurified graphene oxide.[21]

Our results point that GO films are constituted by a layer of 2−3 monolayers of graphene oxide in contact with air and a second layer submerged in the aqueous subphase of small fragments of impurities produced during the oxidation procedure. To confirm this fact, we analyze SNR results of purified graphene oxide in which impurities are eliminated by base washing.

Figure 4a,b shows the experimental SNR results for PGO films at the surface pressure values of 1.8 and 9.9 mN/m, respectively. The SLD used in the fits was 6.85 10^{-6} Å^{-2} and corresponds to graphene oxide of chemical composition:[40] C (85.45), H (%), 0.5 O (14.1%) consistent with XPS results and the density of graphene[53] 2.2 g/cm^3.

Conversely to GO films, the SNR results obtained for PGO films can be well fitted according to a single layer model; see solid lines in Figure 4a,b. This fact is consistent with the removal of impurities and is an additional argument to identify the layer submerged in water in the GO films as oxidation impurities.

The parameters obtained from the fits are listed in Table 2. The SLD profiles across the interface for PGO films at 1.8 and 9.9 mN/m are plotted in Figure 4c,d, respectively. Assuming the existence of a single layer of PGO, the volume fraction was calculated as

Table 2. Parameters Obtained from the Fits for PGO Films[a]

π = 1.8 mN/m		π = 9.9 mN/m	
σ_T/Å	6.50 ± 0.1	σ_B/Å	5.97 ± 0.1
t/Å	14 ± 1	t/Å	18 ± 1
SLD/Å^{-2}	6.85 × 10^{-6}	SLD/Å^{-2}	6.85 × 10^{-6}
ϕ_w	0.76 ± 0.02	ϕ_w	0.79 ± 0.02
σ_B/Å	6.50 ± 0.6	σ_T/Å	5.97 ± 0.4

[a]Errors are reported as absolute values calculated in 1σ interval.

$$\Phi_{PGO}(z) = \frac{1}{2}\phi_{PGO}\left[\mathrm{erf}\left(\frac{z - \frac{t}{2}}{\sqrt{2\sigma_T}}\right) - \mathrm{erf}\left(\frac{z + \frac{t}{2}}{\sqrt{2\sigma_B}}\right)\right] \quad (4)$$

The variation of the volume fraction of PGO values with the distance to the air−water interface calculated from eq 4 and parameters collected in Table 2 are plotted in Figure 4e,f.

The parameters in Table 2 show that the thickness of PGO films decreases compared to the value corresponding to the sheets of the non-purified ones. Moreover, the thickness values obtained from the fits (14 and 18 Å) are consistent with the AFM value of the PGO films on Silicon.[21] As in GO films, the roughness values of PGO exceed the roughness originated only from capillary waves. Therefore, we consider that the PGO layers also produce additional apparent roughness due to the molecular protrusions and orientations at the air/water interface. We observe that the roughness of PGO films is slightly higher than for GO ones. This fact is probably due to the existence of a higher number of protruding corrugations in PGO layers due to the loading of oxygen functional groups.[54] Besides, the roughness of the top and bottom of the layer is the same and almost independent on the surface pressure, that is of the molecular area. The water fraction in the layer, ϕ_w, is almost the same as the value obtained for the top layer of unpurified GO films. The volume fraction of the PGO layer increases with the surface pressure, as expected from the decrease in available molecular area.

Finally, we used the information obtained from SNR to interpret the observed differences between the surface pressure and the compressional elastic modulus isotherms of GO and PGO. As previously discussed, the compressional elastic modulus exhibits two different behaviors for GO and PGO

https://dx.doi.org/10.1021/acsami.0c05649
ACS Appl. Mater. Interfaces 2020, 12, 25453−25463

films, Figure 2c,d. The GO monolayer reaches the collapse at a lower surface pressure than the PGO monolayer. Besides, prior to the collapse, the PGO monolayer is in a state of higher compressional elastic modulus values than the GO monolayer. These facts can be interpreted based on our SNR results. Accordingly, the PGO films are composed of graphene oxide sheets, whereas the GO films are composed of graphene oxide and a second layer of OD submerged in the aqueous subphase. Therefore, as OD is formed by highly oxidized molecules, the sheets of GO are more hydrophilic than the PGO ones, and consequently, they collapse by expulsion at a lower surface pressure.[55] Besides, the more hydrophobic particles, PGO, present lower surface wettability and higher cohesive forces than the GO ones; therefore, they result in a solid-like monolayer with higher compressional elasticity values.[55] Finally, the existence of the second layer in GO films may also be responsible for the increased coverage observed[31] for films of GO transferred from the air−water interface to solids using the LB methodology.

CONCLUSIONS

An in situ model has been proposed to describe the structure of graphene oxide films and the role of OD in the structure and organization of graphene oxide films at the air−water interface. SNR measurements have shown significant differences between graphene oxide and purified graphene oxide films at the air−water interface. All films analyzed in this work correspond to the close-packed region because in this state, the graphene oxide sheets do not overlap each other. Our results demonstrate that GO films are composed of a bilayer in agreement with previous results obtained by X-ray surface scattering.[16] According to our SNR results, the bilayer consists of 2−3 graphene oxide layers stacked in contact with air and a second layer submerged in the aqueous subphase. The results allow us to identify the nature of the second layer as OD which are highly oxidized fragments produced during the oxidation of graphite. In contrast, when the OD fragments are removed, the films of PGO are constituted by one layer in contact with air. As far as we know, this is the first time that the organization of OD has been observed in GO films at the air−water interface. Therefore, we believe that our results can be used to prepare well-controlled graphene oxide thin films to build effective energy devices and sensors. Besides, we also demonstrate that the presence of OD plays an important role in the structure and surface properties of graphene oxide trapped at the air−water interface. We believe that these results are important for various applications in which it is necessary to modulate the properties of GO films to improve the ability of graphene oxide as a foams stabilizer or emulsion stabilizer and to tune its surfactant properties.

AUTHOR INFORMATION

Corresponding Authors

M. Mercedes Velázquez − *Departamento de Química Física, Facultad de Ciencias Químicas, Universidad de Salamanca, 37008 Salamanca, Spain;* orcid.org/0000-0003-2746-8204; Email: mvsal@usal.es

Armando Maestro − *Institut Max von Laue and Paul Langevin, 38042 Grenoble, France;* Email: maestro@ill.fr

Authors

David López-Díaz − *Departamento de Química Física, Facultad de Ciencias Químicas, Universidad de Salamanca, 37008 Salamanca, Spain*

M. Dolores Merchán − *Departamento de Química Física, Facultad de Ciencias Químicas, Universidad de Salamanca, 37008 Salamanca, Spain;* orcid.org/0000-0003-3573-3805

Complete contact information is available at: https://pubs.acs.org/10.1021/acsami.0c05649

Author Contributions

The manuscript was written through contributions of all authors. All authors have given approval to the final version of the manuscript.

Notes

The authors declare no competing financial interest.

ACKNOWLEDGMENTS

The authors thank the Institut Laue-Langevin for allocation of neutron beam time on FIGARO (DOI: 10.5291/ILL-DATA.9-10-1551). We also acknowledge the financial support from European Regional Development Fund, ERDF, Junta de Castilla y León (SA256P18) and MINECO (CTQ2016-78895-R). D.L-D also thanks Junta de Castilla y León for financing his postdoc position. We thank Dr. José Luis García Fierro (Instituto de Catálisis y Petroleoquímica, CSIC, Madrid, Spain) for XPS measurements and the XRD service of University of Salamanca for the XRD measurements. The open access fee was covered by FILL2030, a European Union project within the European Commission's Horizon 2020 Research and Innovation programme under grant agreement N°731096.

ABBREVIATIONS

σ_0, top roughness of the GO layer in contact with air
t_1, thickness of the GO layer in contact with air
ϕ_{w1}, fraction of water in the GO layer in contact with air
σ_1, bottom roughness of the GO layer in contact with air
t_2, thickness of the OD layer submerged in aqueous subphase
ϕ_{w2}, fraction of water in the OD layer submerged in aqueous subphase
σ_2, bottom roughness of the OD layer submerged in aqueous subphase
σ_T, top roughness of the PGO layer
t_{PGO}, thickness of the PGO layer
ϕ_{wPGO}, fraction of water in the PGO layer
σ_B, bottom roughness of the PGO layer

REFERENCES

(1) Wang, X.; Zhi, L.; Mullen, K. Transparent, Conductive Graphene Electrodes for Dye-Sensitized Solar Cells. *Nano Lett.* **2008**, *8*, 323−327.

(2) Wang, X.; Ouyang, Y.; Li, X.; Wang, H.; Guo, J.; Dai, H. Room-Temperature All-Semiconducting Sub-10-nm Graphene Nanoribbon Field-Effect Transistors. *Phys. Rev. Lett.* **2008**, *100*, 206803.

(3) Dimitrakakis, G. K.; Tylianakis, E.; Froudakis, G. E. Pillared Graphene: A New 3-D Network Nanostructure for Enhanced Hydrogen Storage. *Nano Lett.* **2008**, *8*, 3166−3170.

(4) Rodríguez-García, S.; Santiago, R.; López-Díaz, D.; Merchán, M. D.; Velázquez, M. M.; Fierro, J. L. G.; Palomar, J. Role of the Structure of Graphene Oxide Sheets on the CO_2 Adsorption

Properties of Nanocomposites Based on Graphene Oxide and Polyaniline or Fe3O4-Nanoparticles. *ACS Sustainable Chem. Eng.* **2019**, *7*, 12464−12473.
(5) Schedin, F.; Geim, A. K.; Morozov, S. V.; Hill, E. W.; Blake, P.; Katsnelson, M. I.; Novoselov, K. S. Detection Of Individual Gas Molecules Adsorbed On Graphene. *Nat. Mater.* **2007**, *6*, 652−655.
(6) Zhu, Y.; Murali, S.; Cai, W.; Li, X.; Suk, J. W.; Potts, J. R.; Ruoff, R. S. Graphene and Graphene Oxide: Synthesis, Properties, and Applications. *Adv. Mater.* **2010**, *22*, 3906−3924.
(7) Potts, J. R.; Dreyer, D. R.; Bielawski, C. W.; Ruoff, R. S. Graphene-Based Polymer Nanocomposites. *Polymer* **2011**, *52*, 5−25.
(8) Loh, K. P.; Bao, Q.; Eda, G.; Chhowalla, M. Graphene Oxide As A Chemically Tunable Platform For Optical Applications. *Nat. Chem.* **2010**, *2*, 1015−1024.
(9) Prezioso, S.; Perrozzi, F.; Giancaterini, L.; Cantalini, C.; Treossi, E.; Palermo, V.; Nardone, M.; Santucci, S.; Ottaviano, L. Graphene Oxide as a Practical Solution to High Sensitivity Gas Sensing. *J. Phys. Chem. C* **2013**, *117*, 10683−10690.
(10) Mendez-Gonzalez, D.; Calderón, O. G.; Melle, S.; González-Izquierdo, J.; Bañares, L.; López-Díaz, D.; Velázquez, M. M.; López-Cabarcos, E.; Rubio-Retama, J.; Laurenti, M. Contribution Of Resonance Energy Transfer to The Luminescence Quenching of Upconversion Nanoparticles With Graphene Oxide. *J. Colloid Interface Sci.* **2020**, *575*, 119−129.
(11) Singh, R. K.; Kumar, R.; Singh, D. P. Graphene Oxide: Strategies For Synthesis, Reduction And Frontier Applications. *RSC Adv.* **2016**, *6*, 64993−65011.
(12) Staudenmaier, L. Verfahren zur Darstellung der Graphitsäure. *Ber. Dtsch. Chem. Ges.* **1898**, *31*, 1481−1487.
(13) Hummers, W. S.; Offeman, R. E. Preparation of Graphitic Oxide. *J. Am. Chem. Soc.* **1958**, *80*, 1339.
(14) López-Díaz, D.; López Holgado, M.; García-Fierro, J. L.; Velázquez, M. M. Evolution of the Raman Spectrum with the Chemical Composition of Graphene Oxide. *J. Phys. Chem. C* **2017**, *121*, 20489−20497.
(15) Lerf, A.; He, H.; Forster, M.; Klinowski, J. Structure of Graphite Oxide Revisited. *J. Phys. Chem. B* **1998**, *102*, 4477−4482.
(16) De Jesus, L. R.; Dennis, R. V.; Depner, S. W.; Jaye, C.; Fischer, D. A.; Banerjee, S. Inside and Outside: X-ray Absorption Spectroscopy Mapping of Chemical Domains in Graphene Oxide. *J. Phys. Chem. Lett.* **2013**, *4*, 3144−3151.
(17) Martín-García, B.; Velázquez, M. M.; Rossella, F.; Bellani, V.; Diez, E.; García Fierro, J. L.; Pérez-Hernández, J. A.; Hernández-Toro, J.; Claramunt, S.; Cirera, A. Functionalization of Reduced Graphite Oxide Sheets with a Zwitterionic Surfactant. *ChemPhysChem* **2012**, *13*, 3682−3690.
(18) Rozada, R.; Paredes, J. I.; López, M. J.; Villar-Rodil, S.; Cabria, I.; Alonso, J. A.; Martínez-Alonso, A.; Tascón, J. M. D. From Graphene Oxide To Pristine Graphene: Revealing The Inner Workings Of The Full Structural Restoration. *Nanoscale* **2015**, *7*, 2374−2390.
(19) Wang, X.; Zhi, L.; Müllen, K. Transparent, Conductive Graphene Electrodes for Dye-Sensitized Solar Cells. *Nano Lett.* **2008**, *8*, 323−327.
(20) Claramunt, S.; Varea, A.; López-Díaz, D.; Velázquez, M. M.; Cornet, A.; Cirera, A. The Importance of Interbands on the Interpretation of the Raman Spectrum of Graphene Oxide. *J. Phys. Chem. C* **2015**, *119*, 10123−10129.
(21) Rourke, J. P.; Pandey, P. A.; Moore, J. J.; Bates, M.; Kinloch, I. A.; Young, R. J.; Wilson, N. R. The Real Graphene Oxide Revealed: Stripping the Oxidative Debris from the Graphene-like Sheets. *Angew. Chem., Int. Ed.* **2011**, *50*, 3173−3177.
(22) Su, C.; Acik, M.; Takai, K.; Lu, J.; Hao, S.-j.; Zheng, Y.; Wu, P.; Bao, Q.; Enoki, T.; Chabal, Y. J.; Ping Loh, K. Probing The Catalytic Activity of Porous Graphene Oxide and The Origin of This Behaviour. *Nat. Commun.* **2012**, *3*, 1298.
(23) Guo, Z.; Wang, S.; Wang, G.; Niu, Z.; Yang, J.; Wu, W. Effect of Oxidation Debris On Spectroscopic and Macroscopic Properties of Graphene Oxide. *Carbon* **2014**, *76*, 203−211.
(24) Thomas, H. R.; Vallés, C.; Young, R. J.; Kinloch, I. A.; Wilson, N. R.; Rourke, J. P. Identifying The Fluorescence of Graphene Oxide. *J. Mater. Chem. C* **2013**, *1*, 338.
(25) Dimiev, A. M.; Polson, T. A. Contesting The Two-Component Structural Model Of Graphene Oxide And Reexamining The Chemistry Of Graphene Oxide In Basic Media. *Carbon* **2015**, *93*, 544−554.
(26) Chen, X.; Chen, B. Direct Observation, Molecular Structure, and Location of Oxidation Debris on Graphene Oxide Nanosheets. *Environ. Sci. Technol.* **2016**, *50*, 8568−8577.
(27) Cote, L. J.; Kim, F.; Huang, J. Langmuir−Blodgett Assembly of Graphite Oxide Single Layers. *J. Am. Chem. Soc.* **2009**, *131*, 1043−1049.
(28) Kim, J.; Cote, L. J.; Huang, J. Two Dimensional Soft Material: New Faces of Graphene Oxide. *Acc. Chem. Res.* **2012**, *45*, 1356−1364.
(29) Cote, L. J.; Kim, F.; Huang, J. Langmuir−Blodgett Assembly of Graphite Oxide Single Layers. *J. Am. Chem. Soc.* **2008**, *131*, 1043−1049.
(30) López-Díaz, D.; Mercedes Velázquez, M.; Blanco de La Torre, S.; Pérez-Pisonero, A.; Trujillano, R.; Fierro, J. L. G.; Claramunt, S.; Cirera, A. The Role of Oxidative Debris on Graphene Oxide Films. *ChemPhysChem* **2013**, *14*, 4002−4009.
(31) Hidalgo, R. S.; López-Díaz, D.; Velázquez, M. M. Graphene Oxide Thin Films: Influence of Chemical Structure and Deposition Methodology. *Langmuir* **2015**, *31*, 2697−2705.
(32) Roberts, G. G. *Langmuir−Blodgett Films*; Springer Science: Oxford U.K., 1990.
(33) Gilje, S.; Han, S.; Wang, M.; Wang, K. L.; Kaner, R. B. A Chemical Route to Graphene for Device Applications. *Nano Lett.* **2007**, *7*, 3394−3398.
(34) Becerril, H. A.; Mao, J.; Liu, Z.; Stoltenberg, R. M.; Bao, Z.; Chen, Y. Evaluation of Solution-Processed Reduced Graphene Oxide Films as Transparent Conductors. *ACS Nano* **2008**, *2*, 463−470.
(35) Mercedes Velázquez, M.; Alejo, T.; López-Díaz, D.; Martín-García, B.; Dolores Merchán, M. Langmuir-Blodgett Methodology: A Versatile Technique to Build 2D Material Films. In *Two-Dimensional Materials—Synthesis, Characterization and Potential Applications*; Nayak, P. K., Ed.; IntechOpen, 2016; pp 21−42.
(36) Lu, J. R.; Thomas, R. K.; Penfold, J. Surfactant Layers at The Air/Water Interface: Structure and Composition. *Adv. Colloid Interface Sci.* **2000**, *84*, 143−304.
(37) Campbell, R. A.; Saaka, Y.; Shao, Y.; Gerelli, Y.; Cubitt, R.; Nazaruk, E.; Matyszewska, D.; Lawrence, M. J. Structure of Surfactant and Phospholipid Monolayers at The Air/Water Interface Modeled From Neutron Reflectivity Data. *J. Colloid Interface Sci.* **2018**, *531*, 98−108.
(38) Braun, L.; Uhlig, M.; von Klitzing, R.; Campbell, R. A. Polymers and Surfactants at Fluid Interfaces Studied with Specular Neutron Reflectometry. *Adv. Colloid Interface Sci.* **2017**, *247*, 130−148.
(39) Natkaniec, I.; Sheka, E. F.; Drużbicki, K.; Hołderna-Natkaniec, K.; Gubin, S. P.; Buslaeva, E. Y.; Tkachev, S. V. Computationally Supported Neutron Scattering Study of Parent and Chemically Reduced Graphene Oxide. *J. Phys. Chem. C* **2015**, *119*, 18650−18662.
(40) Sheka, E. F.; Natkaniec, I. Neutron Scattering of Parent and Reduced Graphene Oxides. *Rev. Adv. Mater. Sci.* **2017**, *49*, 1−27.
(41) Klechikov, A.; Sun, J.; Vorobiev, A.; Talyzin, A. V. Swelling of Thin Graphene Oxide Films Studied by in Situ Neutron Reflectivity. *J. Phys. Chem. C* **2018**, *122*, 13106−13116.
(42) Bonatout, N.; Muller, F.; Fontaine, P.; Gascon, I.; Konovalov, O.; Goldmann, M. How Exfoliated Graphene Oxide Nanosheets Organize at The Water Interface: Evidence for a Spontaneous Bilayer Self-Assembly. *Nanoscale* **2017**, *9*, 12543−12548.
(43) Smoluchowski, M. V. *Handbuch der Elektrizität und des Magnetismus*; Graetz: Leipzig, 1921; Vol. *11*.
(44) Cubitt, R.; Fragneto, G. Neutron Reflection: Principles and Examples of Applications. In *Scattering*; Pike, R., Sabatier, P., Eds.; Academic Press: London, 2002; Chapter 2.8.3, pp 1198−1208.

https://dx.doi.org/10.1021/acsami.0c05649
ACS Appl. Mater. Interfaces 2020, 12, 25453−25463

(45) Gutfreund, P.; Saerbeck, T.; Gonzalez, M. A.; Pellegrini, E.; Laver, M.; Dewhurst, C.; Cubitt, R. Towards Generalized Data Reduction on a Chopper-Based Time-Of-Flight Neutron Reflectometer. *J. Appl. Crystallogr.* **2018**, *51*, 606−615.
(46) Parratt, L. G. Surface Studies of Solids by Total Reflection of X-Rays. *Phys. Rev.* **1954**, *95*, 359−369.
(47) Gerelli, Y. Aurore: New Software For Neutron Reflectivity Data Analysis. *J. Appl. Crystallogr.* **2016**, *49*, 712.
(48) Huh, S. H. Thermal Reduction of Graphene Oxide.In *Physics and Applications of Graphene-Experiments*; InTech, 2011.
(49) Stankovich, S.; Dikin, D. A.; Piner, R. D.; Kohlhaas, K. A.; Kleinhammes, A.; Jia, Y.; Wu, Y.; Nguyen, S. T.; Ruoff, R. S. Synthesis of Graphene-Based Nanosheets Via Chemical Reduction of Exfoliated Graphite Oxide. *Carbon* **2007**, *45*, 1558−1565.
(50) Thomas, H. R.; Day, S. P.; Woodruff, W. E.; Vallés, C.; Young, R. J.; Kinloch, I. A.; Morley, G. W.; Hanna, J. V.; Wilson, N. R.; Rourke, J. P. Deoxygenation of Graphene Oxide: Reduction or Cleaning? *Chem. Mater.* **2013**, *25*, 3580−3588.
(51) Sinha, S. K.; Sirota, E. B.; Garoff, S.; Stanley, H. B. X-Ray and Neutron Scattering From Rough Surfaces. *Phys. Rev. B: Condens. Matter Mater. Phys.* **1988**, *38*, 2297−2311.
(52) Braslau, A.; Deutsch, M.; Pershan, P. S.; Weiss, A. H.; Als-Nielsen, J.; Bohr, J. Surface Roughness of Water Measured by X-Ray Reflectivity. *Phys. Rev. Lett.* **1985**, *54*, 114−117.
(53) Li, R.; Li, Z.; Pambou, E.; Gutfreund, P.; Waigh, T. A.; Webster, J. R. P.; Lu, J. R. Determination of PMMA Residues on a Chemical-Vapor-Deposited Monolayer of Graphene by Neutron Reflection and Atomic Force Microscopy. *Langmuir* **2018**, *34*, 1827−1833.
(54) Gupta, B.; Kumar, N.; Panda, K.; Kanan, V.; Joshi, S.; Visoly-Fisher, I. Role of Oxygen Functional Groups in Reduced Graphene Oxide for Lubrication. *Sci. Rep.* **2017**, *7*, 45030.
(55) Razavi, S.; Cao, K. D.; Lin, B.; Lee, K. Y. C.; Tu, R. S.; Kretzschmar, I. Collapse of Particle-Laden Interfaces under Compression: Buckling vs Particle Expulsion. *Langmuir* **2015**, *31*, 7764−7775.

https://dx.doi.org/10.1021/acsami.0c05649
ACS Appl. Mater. Interfaces 2020, 12, 25453−25463